

Faraday Discussions

Accepted Manuscript



This manuscript will be presented and discussed at a forthcoming Faraday Discussion meeting. All delegates can contribute to the discussion which will be included in the final volume.

Register now to attend! Full details of all upcoming meetings: <http://rsc.li/fd-upcoming-meetings>



This is an *Accepted Manuscript*, which has been through the Royal Society of Chemistry peer review process and has been accepted for publication.

Accepted Manuscripts are published online shortly after acceptance, before technical editing, formatting and proof reading. Using this free service, authors can make their results available to the community, in citable form, before we publish the edited article. We will replace this *Accepted Manuscript* with the edited and formatted *Advance Article* as soon as it is available.

You can find more information about *Accepted Manuscripts* in the [Information for Authors](#).

Please note that technical editing may introduce minor changes to the text and/or graphics, which may alter content. The journal's standard [Terms & Conditions](#) and the [Ethical guidelines](#) still apply. In no event shall the Royal Society of Chemistry be held responsible for any errors or omissions in this *Accepted Manuscript* or any consequences arising from the use of any information it contains.

Soft repulsive interactions, particle rearrangements and size selection in the self-assembly of nanoparticles at liquid interfaces

Konrad Schwenke^a and Emanuela Del Gado^{*a,b,c}

Received Xth XXXXXXXXXXXX 20XX, Accepted Xth XXXXXXXXXXXX 20XX

First published on the web Xth XXXXXXXXXXXX 200X

DOI: 10.1039/c000000x

In the adsorption of nanoparticles at liquid interfaces, soft and short ranged repulsive effective interactions between the nanoparticles at the interface may eventually induce crowding, slow dynamics and jamming at high surface coverage. These phenomena can interfere with the adsorption process, significantly slowing down its kinetics. Here, by means of numerical simulations, we find that modifying the effective interactions, which can be achieved for example by grafting differently functionalized polymer shells on the bare nanoparticles, may qualitatively change such interplay. In particular our results suggest that, in presence of ultrasoft particle interactions such as the ones described by a Gaussian Core Model potential, a small size polydispersity can be sufficient to decouple the adsorption kinetics from the slow dynamics that develops at the interface, due to a qualitative change from an irreversible adsorption controlled by particle rearrangements at the interface to one dominated by size selection mechanisms. These findings may be useful to achieve higher surface coverages and faster adsorption kinetics.

1 Introduction

The use of nanoparticles as building blocks opens the route to create novel materials, often utilizing their self-assembly into desired patterns. A powerful way for the self-assembly of nanoparticles is to make use of their adsorption at liquid interfaces^{1–3}. The adsorbed particles, in fact, can still move and rearrange within the interface, and made to form various 2-dimensional structures^{1,4–7}. These features are extremely interesting for a wide range of applications ranging from nano-porous filtering devices to nano-scale sensors^{2,8}. In all these cases, a better understanding of the processes involving many particles at the interface is necessary to allow for a better control over material properties. When high coverages and relatively fast self-assembly of the particle-laden interface needs to be achieved, the emerging dynamics of the particles at the interface may affect the adsorption kinetics and the final patterns attained^{9–11}. Collective effects, due to the interactions among many nanoparticles and to their crowding at the interface, are still relatively poorly understood and controlled, requiring deeper and more systematic investigations. The role of the out-of-equilibrium conditions corresponding to the irreversible nature of the adsorption (with typical adsorption strengths which can be of the order of hundreds of $k_B T$ ^{10,12}) is also far from being well rationalized and mastered, in spite of its relevance to achieve the desired performances in the self-assembly process. Elucidating these aspects for well controlled, model systems such as in the case of relatively simple nanoparticles at the classical oil-water

^a Department of Civil, Environmental and Geomatic Engineering, ETH Zurich, Switzerland.

^b Department of Physics and Institute for Soft Matter Synthesis and Metrology, Georgetown University, USA. E-mail: ed610@georgetown.edu

^c Kavli Institute for Theoretical Physics, University of California at Santa Barbara, USA.

or air-water interfaces, is also extremely important to develop the fundamental understanding needed for handling more complex systems, with high potential for new technologies. Examples range from fabrication of droplets with controllable shapes¹³ or bottom-up assembly of smart soft materials^{14–18} to photonic or photovoltaic applications^{19–21}.

This work is aimed at investigating the self-assembly of nanoparticle at liquid interfaces, by means of numerical simulations and a new approach that, in spite of a few simplifications, allows us to account for the irreversible nature of the adsorption process, to follow the adsorption kinetics and to elucidate its interplay with the particle dynamics at the interface. In particular here we focus on how changing the effective interactions from soft to a *ultrasoft* repulsion, which may be achieved in polymer shell nanoparticles but tuning the properties of the polymer brush, may affect and qualitatively change the adsorption of nanoparticles polydisperse in size, a situation quite common in experiments. We gain new insight into the fundamental physical mechanisms controlling the filling of the interface and the emerging dynamics of the adsorbed nanoparticles. In our extended numerical study we consider nanoparticles interacting via an inverse power law potential (IPL) of the form $\sim r^{-n}$ with $n = 12$, widely used as model for short ranged repulsive interactions in liquids and colloidal systems^{22,23}, and via a Gaussian Core Model potential (GCM), which in many cases best reproduces the ultrasoft effective repulsion between polymer shell nanoparticles^{24,25}. We find that, in general, with soft repulsive interactions the adsorption may be slowed down by the crowding of the nanoparticles at the interface, but with ultrasoft repulsive interactions even a relatively small size polydispersity may allow for the adsorption to proceed by size selection, even when the dynamics at the interface is significantly arrested.

The paper is organized as follows. The model and the numerical approach are introduced in Section 2, whereas in Section 3 we analyse the motion of the particles adsorbed at the interface to gain new understanding of the interplay between the particle rearrangements and the adsorption kinetics. In Section 4 we investigate how and when qualitatively different mechanisms can come into play upon making the effective interactions significantly softer and longer ranged. Finally, we discuss and summarize our findings in Section 5.

2 Model and numerical method

We consider nanoparticles interacting at a liquid interface, via soft, short ranged repulsive interactions U . In particular, our study targets polymer shell nanoparticles as in the experiments of Refs.^{9–12,26}: the nanoparticles have an oxide core, whose linear size may vary between 5 and 10nm, and a (PEG) polymer brush grafted on the surface. Depending on the thickness and the grafting density of the polymer brush the overall particle radius may typically vary between 10 and 30 nm. For this type of nanoparticles adsorption strength between 10^2 and $10^3 k_B T$ have been measured or estimated^{10,12,27,28}. The polymer brush is typically used to stabilize the particle assembly at the interface against aggregation by screening the attraction between the cores, so that a relatively steep and short range repulsion is expected to dominate the particle-particle effective interactions at the interface. To model these interactions, we use an inverse power law (IPL) potential:

$$U_{ij} = \varepsilon(\sigma/r_{ij})^{12} \quad (1)$$

where r_{ij} is the distance between particles i and j , σ is the particle diameter and the interaction potential is cut off at $r_c = 2.5\sigma$. IPL has the advantage of being a widely studied (therefore convenient and sufficiently general) case^{22,23,29}. Its phase diagram can be characterized by a single control parameter $\hat{\Gamma} = (\phi/4\pi)T^{-1/6}$ where ϕ is the total area coverage. This choice allows us to more directly compare our simulations with studies existing in the literature and using different values of the temperature T and/or coverage ϕ .

It has been shown that when the polymer chains are quite long and the grafting density of the brush is not too high, significant conformational changes of the polymers at the interface are possible, and the effective particle interactions may qualitatively change, becoming more similar to a Gaussian profile^{24,30}. To model

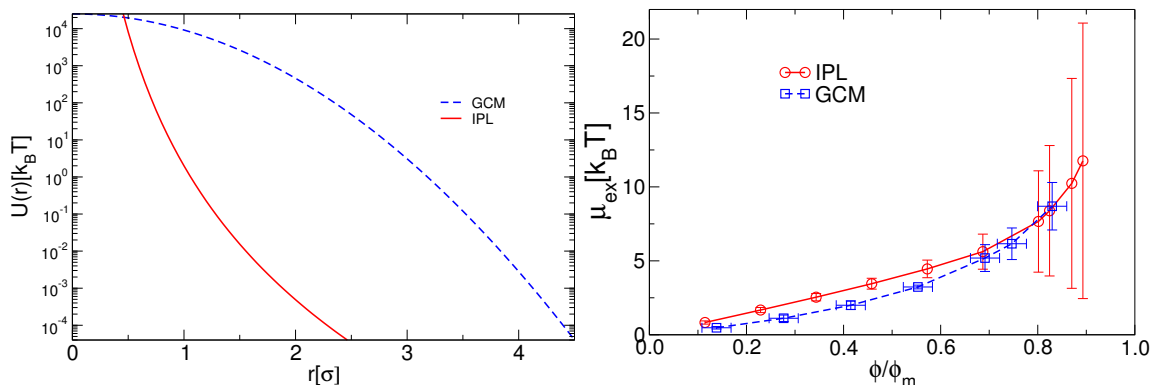


Fig. 1 Left: Interaction potential IPL and GCM as a function of the distance between particles. Right: Excess chemical potential as function of the distance ϕ/ϕ_m from the melting point for power-law and Gaussian potential with the parameters used in this study.

this type of *ultrasoft* interactions, we use the Gaussian Core Model (GCM)

$$U_{ij} = 500\epsilon \exp\left[-(r_{ij}/\sigma)^2\right] \quad (2)$$

cut-off at $r_c = 5\sigma$. The relatively more complex phase diagram of this type of potential, featuring for example a reentrant melting upon increasing density, has been studied in several works^{31–37}. In our simulations both potentials are shifted so that $U(r_c) \simeq 0$ and we use reduced units, with all lengths given in terms of σ and ϵ being the unit energy. The difference in the shape of the two interaction potentials is shown in Fig. 1(left).

We have designed a Monte Carlo (MC) scheme to mimic the adsorption of the nanoparticles to an interface. Typical liquid interface thicknesses at room temperature are of the order of a few Angstroms^{38,39}, hence the interface is a sharp boundary between the two phases. The nanoparticle adsorption energy ΔE can be, to a first approximation, taken proportional to the square of the particle diameter and is fixed by the chemistry of the nanoparticles and the fluids⁴⁰. We model the interface as a flat, 2D simulation box with periodic boundary conditions and assume that diffusion within the interface is much slower than in the bulk^{41,42} (adsorbed particles are added instantaneously to the interface). The acceptance probability for adding or removing a new particle to/from the simulation box is given by $\min[1, e^{\pm\beta(\Delta E - U)}]$, with U being the repulsion from the particles already present at the interface and $\beta = 1/k_B T$. This MC approach can be seen as a Grand Canonical Monte Carlo scheme^{43–45} where the adsorption free energy per particle ΔE represents the main contribution to the excess part of the chemical potential¹¹. In the Grand Canonical Monte Carlo the excess chemical potential would contain the additional term due to the particle-particle interactions at the interface, which changes with the particle density. In Fig. 1(right) this excess chemical potential due to the particle-particle interactions in absence of adsorption, computed using the Widom insertion method^{46,47}, is plotted for IPL and GCM for the same temperature, interactions and simulation box size of interest here. The data show that this contribution increases with density but the related increase is, in a first approximation, negligible with respect to the typical adsorption energies of the nanoparticles at oil-water or air-water interfaces ($\Delta E > 100k_B T$)^{12,27,28}. Hence we don't expect significant differences when using the Grand Canonical Monte Carlo scheme.

We also include size polydispersity, which is always present in samples of synthesized nanoparticles. For the polydisperse samples we use a Gaussian size distribution with mean value $\langle\sigma_i\rangle = 1.0\sigma$ and standard deviation 0.15, a value which is typical of experimental nanoparticle batches^{10,11,26}. The size distribution is truncated for practical reasons at 0.7σ and 1.3σ . Differently from most studies of polydisperse systems

where the chemical potential $\mu_{ex}(\sigma_i)$ is adjusted to obtain a prescribed size distribution in the simulation box⁴⁸, here the distribution of particle sizes in the bulk $p(\sigma_i)$ is assigned and we focus on the effect of the adsorption energy that depends on the particle size. Hence, the acceptance rate of an adsorption/desorption attempt, $acc(N \rightarrow N + 1)$ or $acc(N + 1 \rightarrow N)$, depends on $\Delta E(\sigma_i)$. To guarantee microscopic reversibility for each particle size σ_i , we have suitably modified the acceptance probabilities in the MC scheme to account for the fact that the size distribution $p_{int}(\sigma_i)$ at the interface will differ from $p(\sigma_i)$ as the adsorption proceeds. With particles polydisperse in size the interaction energy depends on the diameter of the interacting particles σ_i and σ_j via $\sigma_{ij} = (\sigma_i + \sigma_j)/2$. The adsorption energy in this case is $\Delta E = -\Delta E_0(\sigma_i/\sigma)^2$ where ΔE_0 is fixed by the chemistry of the nanoparticles and the fluids. We use $\Delta E_0 = 200k_B T$ in the simulations, hence the adsorption strength varies between $\simeq 100k_B T$ and $\simeq 350k_B T$ in the polydisperse samples. These values guarantee that the adsorption is irreversible (i.e., we do not observe any spontaneous desorption of particles during the simulations) and are consistent with the findings of experiments for the type of nanoparticles we are interested in here^{10,12,27}.

We consider that the interplay between the adsorption of nanoparticles from the bulk and the dynamics of the particles within the interface is governed essentially by two characteristic time scales. The first one is the typical time τ_a between successive adsorption of particles, which is expected to decrease with the concentration of nanoparticles in the bulk and sets the adsorption rate $\Gamma \simeq \tau_a^{-1}$. To a first approximation, the other relevant time scale in the problem is given by the characteristic relaxation time of the particles dynamics at the interface $\tau_{rel}(\phi)$, which increases with increasing the interface coverage ϕ . The dynamics of the particles adsorbed at the interface, and interacting via IPL or GCM, is investigated here by means of Molecular Dynamics (MD) or Langevin dynamics (LD). For the adsorption we alternate MC cycles with MD runs, with each MC cycle consisting of N_0 attempts to adsorb or desorb a particle. N_0 accounts for the dependence of the adsorption rate on the particle concentration in the bulk and in the following we use $N_0 = 3 \cdot 10^3$ for IPL and $N_0 = 2 \cdot 10^5$ for GCM. Varying the number of MC cycles per total elapsed MD time allows us to change the adsorption rate Γ . Given $\tau = \sqrt{m\sigma^2/\varepsilon}$ the unit time in the MD runs (m is the unit mass of each nanoparticle), we use $\Gamma = 50\tau^{-1}$ to model fast irreversible adsorption and $\Gamma = 0.02\tau^{-1}$ for the limit of slow, reversible adsorption.

It is important to note that the simulations reported here do not include the Brownian dynamics nor the hydrodynamics at the interface, making it impossible to quantitatively match the experimental time scales. A more complete and realistic description of the particle dynamics at the interface is far from trivial for large system sizes as the ones of interest here and is the subject of ongoing work. Nevertheless we have adjusted the characteristic time scale of the particle dynamics at the interface with respect to the adsorption rate Γ so that the simulated adsorption process is qualitatively similar to the reference experiments in Refs.^{10,11}, by setting the reduced temperature T to 0.5ε for IPL and 0.02ε for GCM, respectively. In general, changing T allows us to adjust the characteristic time scale of the particle dynamics at the interface (i.e., for a fixed coverage, decreasing the temperature will slow down the dynamics). With the choices made here, for monodisperse samples of IPL and GCM particles we observe a slowing down of the adsorption kinetics upon densification of the interface, qualitatively similar to the one reported in Refs.^{10,11} and occurring between 10 and 10^3 s. We then introduce the size polydispersity and analyze the possible origin of the deviations from the reference behavior.

For all simulations discussed in the following we used 20 independently generated samples and we computed sample-to-sample fluctuations to estimate the error bars. In each sample we used a number of particles ranging between 2800 and 6000. The size of the simulation boxes was set to $L = 70\sigma$ for the IPL systems and to $L = 200\sigma$ for the GCM. In the MD runs the temperature is controlled with a Nosé-Hoover thermostat^{47,49} and we use an integration time step $\delta t = 0.004\tau$. After each particle insertion MC cycle, we use a smaller step ($8 \cdot 10^{-7}\tau \leq \delta t \leq 0.004\tau$) to reduce temperature fluctuations.

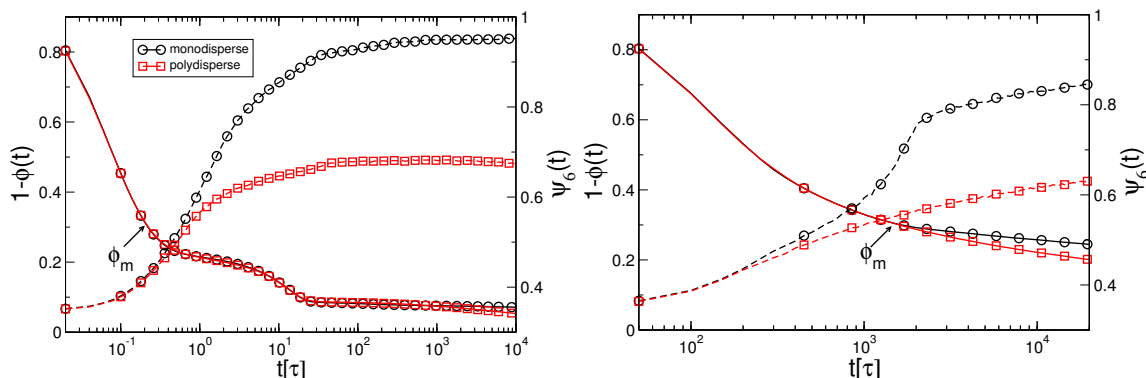


Fig. 2 $1 - \phi(t)$ for monodisperse (black) and polydisperse systems (red) interacting with the IPL-potential and their bond orientational order parameter $\langle \Psi_6 \rangle$, with $\Gamma = 50\tau^{-1}$ (left) and $\Gamma = 0.02\tau^{-1}$ (right).

3 Soft repulsive interactions, crowding and particle motion at the interface

We used the approach described above to investigate the adsorption of nanoparticles interacting via the soft repulsive potential IPL in Ref. ¹¹.

In the experiments ^{10,50}, the evolution of the surface coverage with time is quantified in terms of the progressive decrease, over time, of an *apparent* interfacial tension $\gamma(t)$ of the particle laden interface with respect to the equilibrium interfacial tension γ_0 of the bare liquid interface. Due to the irreversible nature of the particle adsorption at the interface in these experiments, $\gamma(t)$ is an intrinsically non-equilibrium property of the system ⁵¹. Nevertheless, assuming that at each measurement step the particle laden interface is in mechanical equilibrium, $\gamma(t)$ can still be operationally defined and measured reproducibly. To a first approximation, neglecting particle-particle interactions at the interface, $\gamma_0 - \gamma(t)$ can be taken as linearly dependent on the adsorption strength and on the number of particles, per unit area, adsorbed at the interface at each step of the measurement. This number is given by $4\phi(t)/\pi\sigma^2$, where $\phi(t)$ is the fraction of the surface covered by particles. Hence $\gamma(t)$ can be, to a first approximation, related to the particle surface coverage $\phi(t)$ as $\gamma(t)/\gamma_0 \propto 1 - \text{const} \cdot \phi(t)$ (see also the Supplementary Information of Ref. ¹¹). In the following we therefore analyse the adsorption kinetics in terms of the surface coverage measured in the simulations as $\phi(t) = \sum_i \pi\sigma_i^2/4L^2$ (where the sum runs over all the particles residing at the interface). Fig. 2 summarizes the main findings in terms of $1 - \phi(t)$ and of the average hexatic order parameter $\langle \Psi_6 \rangle$ of the particle configurations as a function of time. $\langle \Psi_6 \rangle$ quantifies the degree of order around each particle k adsorbed at the interface, starting from $\Psi_{6k} = \frac{1}{N_k} \sum_{j=1}^{N_k} \exp(i6\Theta_{jk})$, where the sum is taken over all the N_k neighbors of particle k and Θ_{jk} is the angle of the bond connecting particles j and k ⁵². $|\Psi_{6k}|$ is 1 if the particle is in a perfect hexagonal environment and goes to 0 otherwise. We use the average over all particles $\langle \Psi_6 \rangle = \frac{1}{N} \sum_{k=1}^N |\Psi_{6k}|$ as a measure for the overall degree of orientational order in the system. The left panel of Fig. 2 shows the data obtained in the case of fast adsorption ($\Gamma = 50\tau^{-1}$), where we observed that, upon increasing the surface coverage, the adsorption slows down and $1 - \phi(t)$ develops a pseudo-plateau before continuing further, very similar to what observed in the experiments of Refs. ^{10,11}. In the simulations we find that the order at the interface increases significantly over the pseudo-plateau, and that the progressive ordering creates voids which eventually allow for further particle uptake ¹¹. This phenomenon is clearly controlled by the adsorption rate: when the adsorption is sufficiently slow, the surface coverage continuously increases without the slowing down associated to the pseudo plateau, as shown in the right panel of Fig. 2. Interestingly enough, the presence of size polydispersity for the nanoparticles does not seem to modify the adsorption kinetics just described. The same was found in experiments with controlled size polydispersity ¹¹. The dependence of the pseudo-plateau on the adsorption

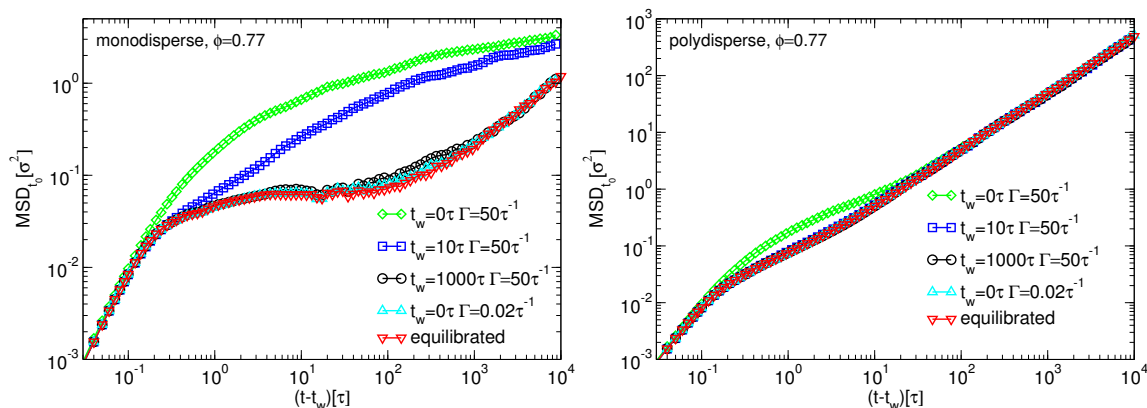


Fig. 3 Mean squared displacement for monodisperse (left) and polydisperse systems (right) interacting with IPL, where adsorption was stopped at $\phi \simeq 0.77$, after different waiting times t_w and different Γ as well as for equilibrated systems.

rate indicates that its origin lies in the interplay between the time scale naturally associated to the adsorption (i.e., the adsorption rate controlled mainly by the density of nanoparticles in the bulk and their mobility in the solvent in which they are immersed) and the characteristic time scales of the particles motion once they are adsorbed at the interface. To further elucidate this point, here we have investigated the time correlations in the particle displacements at the interface for specific values of the surface coverages reached upon adsorption. In particular, we interrupt the adsorption (i.e., the MC cycles) at a time $t_0(\phi)$ (in terms of the elapsed MD time) at which a specific surface coverage ϕ is attained and let the particles adsorbed so far evolve with standard NVT MD (or Langevin dynamics). For a fixed ϕ , starting from the configuration obtained at $t_0(\phi)$, we compute the particle mean squared displacement

$$MSD_{t_0}(t - t_w) = N^{-1} \sum_{k=1}^N [\mathbf{r}_k(t) - \mathbf{r}_k(t_w)]^2 \quad (3)$$

where $\mathbf{r}_k(t)$ denotes the position of particle k at time t , the sum runs over all the particles at the interface and t_w , varying from 0 to 1000τ , is the MD time elapsed between the interruption of the adsorption and the beginning of the measurement. First we analyse the aging of the particle dynamics upon varying t_w . Fig. 3 shows the $MSD_{t_0}(t - t_w)$ for mono- and polydisperse systems at $\phi \simeq 0.77$, corresponding to the onset of the pseudo-plateau, left to age for different t_w after adsorption was stopped at the corresponding $t_0(\phi)$. The data refer to $t_w = 0$, $t_w = 10\tau$ and $t_w = 1000\tau$ as the waiting times. We notice that for the monodisperse samples the plateau in the $MSD_{t_0}(t - t_w)$ becomes far more pronounced upon aging, indicating that the time correlations in the particle motion, measured right after adsorption has been stopped, are qualitatively different from the equilibrium supercooled dynamics, measured at the same coverage without adsorption or when the adsorption is sufficiently slow. The polydisperse samples clearly display a much reduced aging and a weaker particle localisation, as expected⁵³. Nevertheless, the time scale associated to the onset of the pseudo plateau in the adsorption kinetics (i.e., $t \simeq 1 - 10\tau$) corresponds in both cases (monodisperse and polydisperse) to a subdiffusive regime in the particle dynamics at the interface, suggesting that in both cases the slowing down of the particle dynamics at the interface due to crowding is responsible for the slowing down of the adsorption kinetics.

Fig. 4 displays instead the $MSD_{t_0}(t)$ computed for monodisperse (left) and polydisperse particles (right) immediately after adsorption was stopped at $t_0(\phi)$ (i.e., $t_w = 0$), upon varying the surface coverage ϕ . For monodisperse particles we find that for $\phi > 0.70$ the long time diffusive behaviour is not reached anymore over the simulation time window. The $MSD_{t_0}(t)$, in fact, shows an extended subdiffusive time dependence

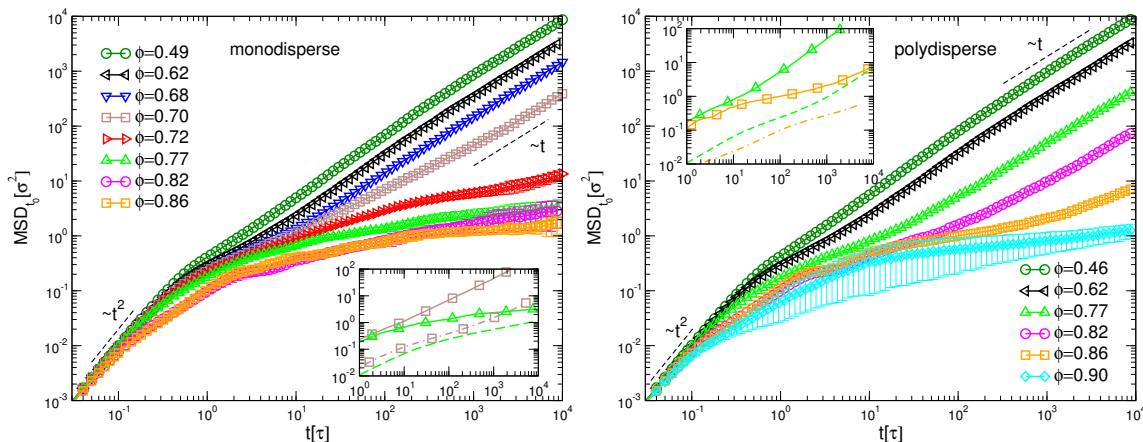


Fig. 4 $MSD_{t_0}(t)$ for monodisperse (left) and polydisperse (right) IPL samples where the adsorption ($\Gamma = 50\tau^{-1}$) was stopped at different ϕ (measured at $t_w = 0$). Insets: Comparison of between NVT simulations (symbols) and Langevin Dynamics (lines) for $\phi \simeq 0.77$ (dashed), $\phi \simeq 0.70$ (dot-dashed, monodisperse) and $\phi \simeq 0.86$ (dot-dashed, polydisperse).

at long times, as in structurally arrested systems^{54,55}. The inset of the Figure shows a comparison, at $\phi = 0.70$ and $\phi = 0.77$, between the $MSD_{t_0}(t)$ measured in NVT MD runs (symbols) and in Langevin Dynamics runs (dashed lines) performed with a friction coefficient $\gamma = 100\tau^{-1}$, indicating that this relatively sharp transition does not depend on the particle motion at short times⁵⁶. For the polydisperse samples we observe instead that, although the adsorption kinetics seems to be unaltered, the particle motion is quite different: the $MSD_{t_0}(t)$ always reaches a diffusive regime at long times (over a time increasing with ϕ), even at quite high surface coverages. These findings are consistent with recent experimental observations for polydisperse particle samples⁷. They suggest that in the IPL systems even a relatively weak crowding, not necessarily associated to structural arrest of the particle assemblies at the interface, may have a significant effect on the adsorption kinetics.

Further insight is obtained by quantifying the deviation from a Gaussian distribution for the particle displacements in terms of the non-Gaussian parameter⁵⁷

$$\alpha_{2,t_0}(t-t_w) = \frac{N^{-1} \sum_{i=1}^N [\mathbf{r}_i(t) - \mathbf{r}_i(t_w)]^4}{2 \left(N^{-1} \sum_{i=1}^N [\mathbf{r}_i(t) - \mathbf{r}_i(t_w)]^2 \right)^2} - 1, \quad (4)$$

with $\alpha_{2,t_0}(t-t_w) = 0$ for a Gaussian distribution of particle displacements. In supercooled liquids, $\alpha_{2,t_0}(t-t_w)$ typically displays a maximum which marks the characteristic time scale of cooperative dynamical processes responsible for the slowing down of the dynamics and eventually decays to 0. The maximum height increases upon approaching structural arrest in model supercooled liquids based on a similar IPL potential^{54,58}. In Fig. 5 (left), we plot $\alpha_{2,t_0}(t-t_w)$ for polydisperse systems at $\phi \simeq 0.77$, for different values of t_w and adsorption rate Γ . The data show that at long times the subdiffusive behaviour in the $MSD_{t_0}(t-t_w)$ is associated to a peak of $\alpha_{2,t_0}(t-t_w)$, very similar to standard supercooled liquids⁵⁹⁻⁶¹. The peak becomes broader and lower with increasing ϕ ⁵⁹. Similar features, only with higher values of $\alpha_{2,t_0}(t-t_w)$, are detected for the monodisperse samples (not shown). Interestingly enough, $\alpha_{2,t_0}(t-t_w)$ also shows a distinct, pronounced peak at very short times (see inset), indicating that not only the crowding at the interface may affect the adsorption kinetics but also that, in turn, the non-equilibrium conditions created by the adsorption kinetics may significantly affect the particle dynamics at the interface. Fig. 5 (right)) shows that the height of this short-time peak is negligible at low enough coverages (i.e., when the interface is not crowded yet), it is maximum close to the onset of

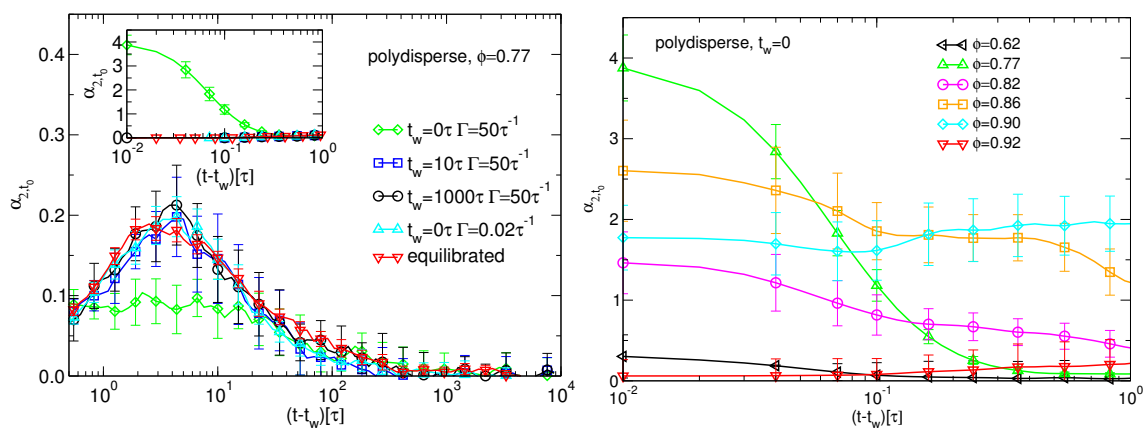


Fig. 5 Non-Gaussian parameter $\alpha_{2,t_0}(t - t_w)$ for IPL systems. Left: Polydisperse systems where adsorption was stopped at $\phi \simeq 0.77$ after different waiting times t_w and different Γ as well as for equilibrated systems. Inset: short-time dynamics. Right: Polydisperse systems at different ϕ , directly after adsorption was stopped.

the pseudo-plateau and eventually decreases with increasing ϕ . These observations suggest that, once the interface get crowded and locally ordered domains start to grow, the non-Gaussianity that we detect right after adsorption might be due to newly adsorbed particles whose number decreases with increasing ϕ .

To analyze more quantitatively how the adsorption process changes the particle motion at the interface, we monitor the $MSD_{t_0,a}(t)$ of the particles while new particles are being adsorbed. In Fig. 6 we plot the mean squared displacement measured during the adsorption of new particles starting from a surface coverage $\phi = 0.77$ (with the high adsorption rate $\Gamma = 50\tau^{-1}$), i.e., at the onset of the plateau. The data refer to the monodisperse samples, but qualitatively the same behaviour is observed also for the polydisperse ones. The new particle uptake at the end of the pseudo-plateau (indicated by the central arrow in the Figure) corresponds to a superdiffusive time dependence of the $MSD_{t_0,a}(t)$. Such dependence is associated to a strongly non-Gaussian distribution of the particle displacements, as shown in the right panel of the Figure, and is the consequence of the particle uptake avalanche triggered by the increase of the local orientational order over the pseudo-plateau (see Fig.2 (left)). These findings are somewhat reminiscent of the avalanche mediated crystallisation detected in⁶², but here they seem to be directly related to the ongoing adsorption rather than to the crystallisation, since the same is observed in the polydisperse samples. The non-Gaussianity of the particle displacements persist at higher coverages, when adsorption is progressively slower and the overall particle motion at the interface is severely hindered, suggesting that the particle motion in the very slow regime of the adsorption kinetics has the character of small avalanches triggered by the rare adsorption events.

4 From soft to ultrasoft: adsorption, jamming and size selection with the Gaussian Core Model

After having gained some new insights into the fundamental physical mechanisms controlling the interplay between the fast, irreversible adsorption and the interface crowding, we now investigate the effect of ultrasoft particle interactions at the interfaces, such as the ones that can arise in the case of core-shell nanoparticles, where the shell is a thick, soft polymer brush grafted on the bare nanoparticle²⁴. To this aim, we applied the numerical approach described in Section 2 to nanoparticles interacting via the GCM potential. In Fig. 7 we plot $(1 - \phi(t))$ and $\psi_6(t)$ obtained in these simulations. Also in this case we observe the emergence of the pseudo-plateau in the monodisperse case if adsorption happens sufficiently fast. As found with IPL, $\psi_6(t)$

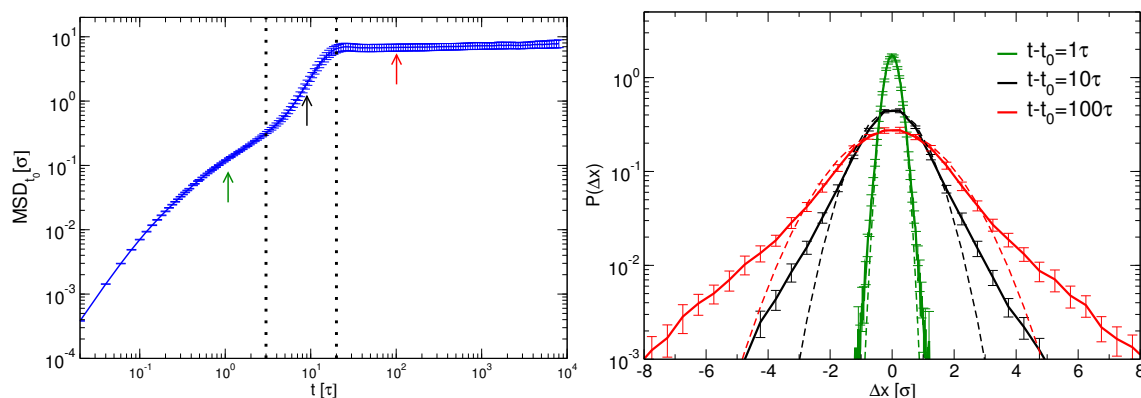


Fig. 6 Left: $MSD_{t_0,a}(t)$ with ongoing adsorption starting from $\phi = 0.77$, with $\Gamma = 50\tau^{-1}$ (monodisperse samples). The dashed black lines indicate the end of the pseudo-plateau in the particle adsorption and the end of the second particle uptake, respectively. Right: Distributions of particle displacements at times corresponding to the arrows in the left panel. The dashed lines are Gaussian distributions obtained by fitting the whole set of data ($t_0 = 1\tau$) or the central part.

indicate a significant increase of the local order at the interface over the time scale of the pseudo-plateau. As already mentioned in Section 2, for the sake of comparison, we have tuned the parameters of the simulations (N_0 and T) and made the time-scale over which the pseudo-plateau appears in the GCM systems comparable to the one obtained with the IPL by choosing a larger N_0 and a lower T . Similarly to the IPL case, decreasing the adsorption rate makes the pseudo-plateau progressively disappears. These similarities suggest that the same mechanisms should be at work in the case of both potentials. Nevertheless we detect striking differences once we consider the polydisperse samples. The same amount of polydispersity used in the case of IPL now qualitatively changes the adsorption curve: the pseudo plateau disappears and the adsorption is significantly faster, leading to higher coverages (with respect to the monodisperse samples), in spite of the fact that the increase in the local orientational order at the interface is still qualitative similar to the one detected in the IPL samples (see Fig. 2 for comparison).

Fig. 8 displays a representative set of snapshots obtained from the simulations for the IPL and GCM samples (monodisperse and polydisperse), at coverages that correspond to the end of the pseudo-plateau, i.e. $\phi \simeq 0.82$ for IPL and $\phi \simeq 0.0924$ and $\phi \simeq 0.0975$ for GCM. The color code is given by the value of local ψ_6 , computed for each particle. Whereas the monodisperse samples have extremely similar patterns, we can detect a qualitative difference between IPL and GCM for the polydisperse ones, in that, although the samples are overall disordered for both potentials, the spatial extent of locally ordered domains is consistently reduced with GCM. For the IPL systems the growth of the locally ordered domain was found to be the mechanism allowing for the new particle uptake at the end of the pseudo-plateau, hence this finding supports the idea that the interplay between adsorption kinetics and dynamic processes at the interface might change qualitatively in presence of ultrasoft effective interactions between the nanoparticles.

To deeper investigate this issue we analyse the particle displacements at the interface at different degrees of coverages reached at a time $t_0(\phi)$ in simulations with a high adsorption rate ($\Gamma = 50\tau^{-1}$). In Fig. 9 the mean squared displacement $MSD_{t_0}(t - t_w)$ computed after stopping the adsorption at $\phi \simeq 0.0907$, i.e., at the onset of the pseudo-plateau, is plotted as a function of the elapsed time and for different values of t_w . The comparison of the left and the right panels with Fig. 3 indicates that the localisation of the particle motion at the interface is overall stronger with respect to the IPL samples. The evolution towards the equilibrium supercooled (or arrested) dynamics seems to be slightly faster upon adding polydispersity, consistently with what observed with IPL. Nevertheless it is striking that the same amount of polydispersity with GCM is not sufficient to fluidize significantly the samples and we do not observe any long time diffusive behaviour.

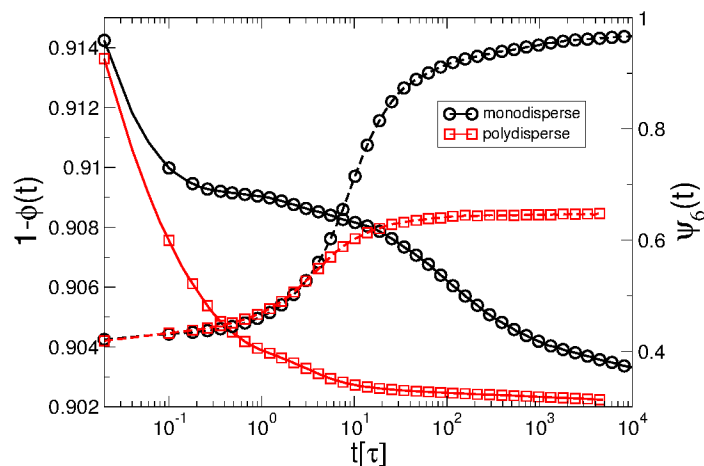


Fig. 7 $1 - \phi(t)$ (full lines) for monodisperse (black) and polydisperse systems (red) interacting with a Gaussian potential and the bond orientational order parameter $\langle \psi_6 \rangle$ (dashed) for systems with $\Gamma = 50\tau^{-1}$.

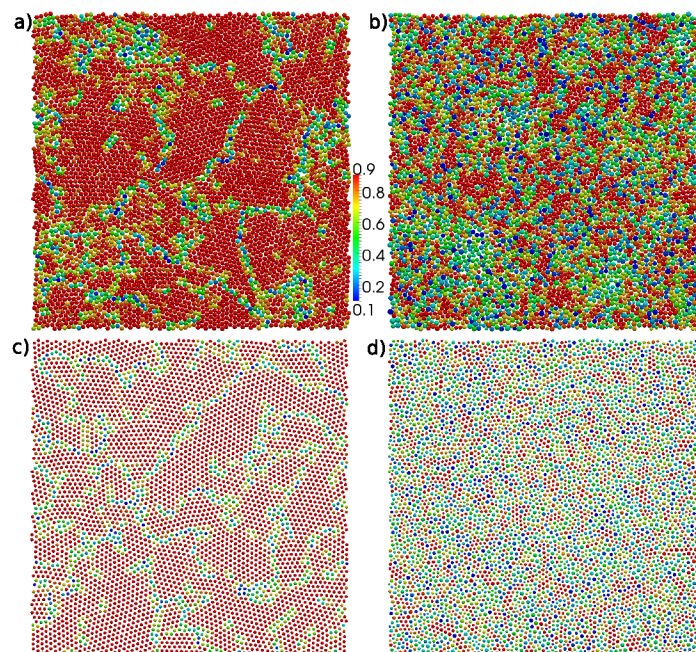


Fig. 8 Snapshots where the color code (see bar in the figure) indicates the value of ψ_6 for IPL systems at $\phi \simeq 0.82$ (a and b) and GCM systems (c and d) at $\phi \simeq 0.0924$ (c) and $\phi \simeq 0.0975$ (d), respectively. Those coverages correspond to states at which $\langle \psi_6 \rangle$ has increased significantly. The images on the left are from monodisperse systems and the ones on the right from polydisperse ones. For the GCM systems the particles are displayed with diameter $2\sigma_i$ for better visibility.

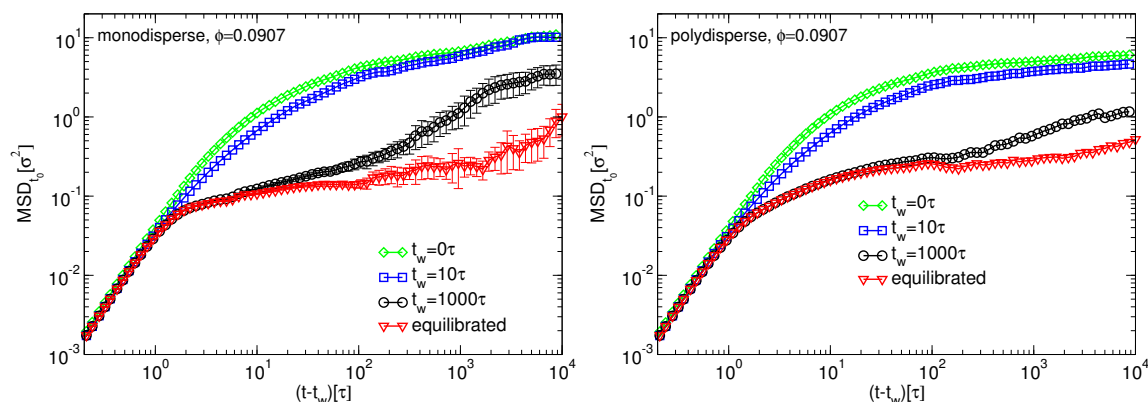


Fig. 9 Mean squared displacement for monodisperse (top) and polydisperse GCM systems (bottom), where adsorption was stopped at $\phi \simeq 0.0907$, after different waiting times t_w .

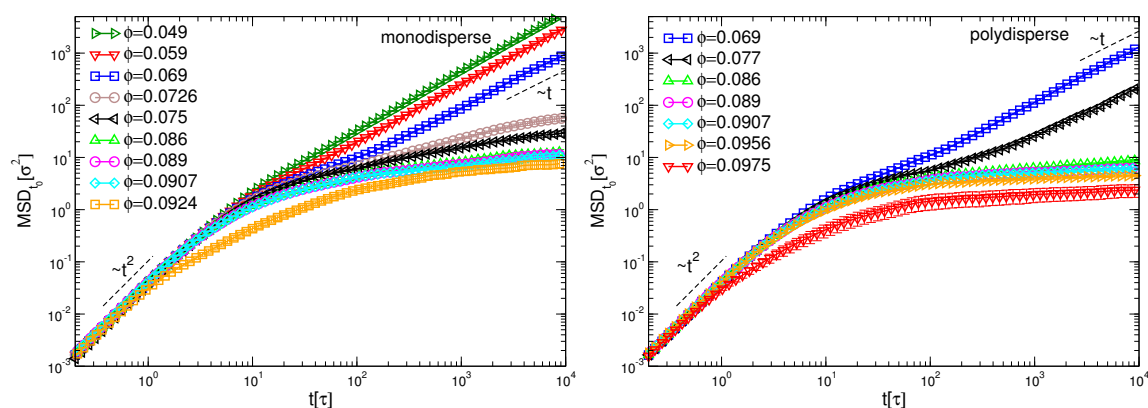


Fig. 10 Mean squared displacement for monodisperse (left) and polydisperse (right) systems interacting with the Gaussian potential where adsorption ($\Gamma = 50\tau^{-1}$ and $N_0 = 2 \cdot 10^5$) was stopped at different ϕ .

This fact could be understood considering that the coverages needed to develop the pseudo-plateau regime in the adsorption kinetics with GCM corresponds to particle configurations that are more deeply quenched and closer to structural arrest, so that a much larger polydispersity would be required to qualitatively change the particle dynamics at the interface. Interestingly the same amount of polydispersity is enough to change the adsorption kinetics and make the pseudo-plateau disappear.

This picture is confirmed when we plot $MSD_{t_0}(t - t_w)$ computed at $t_w = 0$ after having interrupted the adsorption at different coverages ϕ , shown in Fig. 10. The data indicate that at lower coverages, i.e., before reaching the pseudo-plateau in the adsorption curve of Fig. 7, the fluidizing effect of the polydispersity is apparent. At the coverages at which the pseudo-plateau sets in for the monodisperse samples, the particle motion is instead significantly arrested and this feature is not significantly modified in presence of size polydispersity. In Fig. 11, the non-Gaussian parameter $\alpha_{2,t_0}(t - t_w)$ computed when the adsorption is interrupted at the onset of the plateau and for different t_w is shown. The left and right panel refer, respectively, to monodisperse and polydisperse samples. In agreement with what discussed so far, at these coverages the

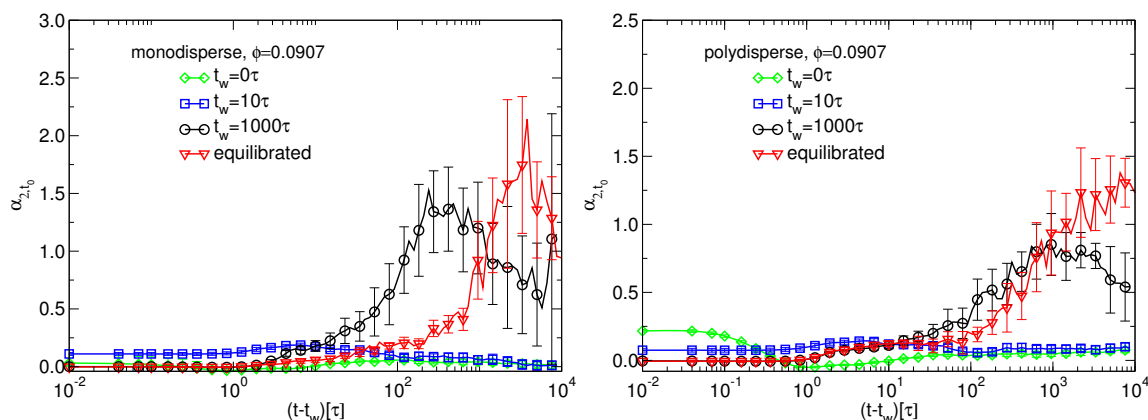


Fig. 11 Non-Gaussianity parameter $\alpha_2(t)$ for monodisperse (top) and polydisperse (bottom) GCM systems, where adsorption was stopped at $\phi = 0.0907$, after different waiting times t_w .

non-Gaussian parameter indicates that the particle configurations are relatively close to structural arrest, with the maximum appearing over time scales of the order of the simulation time window and the value of the maximum being quite higher than the one detected for the IPL samples at the onset of the pseudo-plateau. This last observation is even more striking if one considers that with GCM one would in principle expect less pronounced dynamical heterogeneities due to the longer range of the interactions^{33,63}. The height and the position of the maximum in the non-Gaussian parameter remains qualitatively the same in the polydisperse samples. Interestingly enough, $\alpha_{2,t_0}(t - t_w)$ is different from 0 at short times for small t_w , a feature reminiscent of the short-time non-Gaussianity detected in the IPL samples (Fig. 5), but here its value is significantly reduced and negligible with respect to the long-time one associated to the glassy structural arrest detected also at the same surface coverages without adsorption. Hence GCM systems are comparatively closer to structural arrest but the particle motion at the interface seems to be less prone to be affected by the fast irreversible adsorption. This conclusion is supported by the data shown in Fig. 12, where we plot the mean squared displacement $MSD_{t_0,a}(t)$ and the distributions of the particle displacements computed with ongoing adsorption, starting at coverages at the onset of the pseudo-plateau, in the monodisperse GCM samples. The numerical results indicate that, differently from what observed for the IPL samples in Fig. 6, the second uptake of particles at the end of the plateau has the only effect of progressively arresting the particle motion, as expected when increasing the surface coverage, without producing avalanches in the particle displacements. Consistently, the distributions of particle displacements plotted in the right panel keep their Gaussian shape. The comparison of these data with the ones of Fig. 6 elucidates how the anomalous particle displacements detected for the IPL samples are indeed a feature of the combined effect of the adsorption kinetics with the interparticle interactions, which can be qualitatively changed by introducing ultrasoft interactions.

In spite of a few new insights, the emerging picture for the interplay between the particle dynamics at the interface and the adsorption kinetics for GCM systems is somewhat contradictory. On the one hand, the study of the particle motion at the interface indicates that they are less prone to be affected by the out-of-equilibrium adsorption and therefore suggests a weaker coupling between the GCM particle assemblies and the adsorption kinetics at the interface. On the other, a small size polydispersity seems to be sufficient to qualitatively change the adsorption kinetics. This apparent contradiction suggests that different mechanisms come into play in the formation of the particle laden interface in presence of the ultrasoft interactions. To further investigate this issue we plot in Fig. 13 the size distribution of the particles inserted within prescribed time intervals during ongoing adsorption for IPL and GCM polydisperse samples. The inset shows the size distribution of

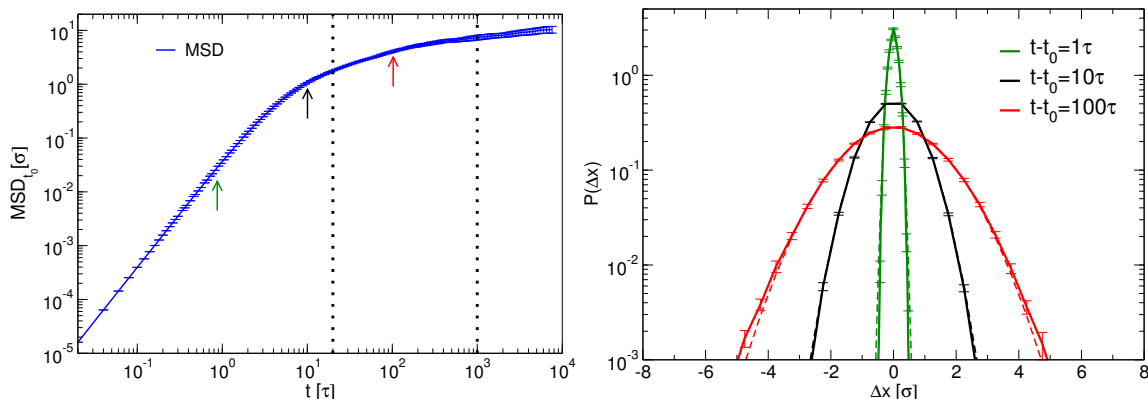


Fig. 12 Left: $MSD_{t_0,a}(t)$ with ongoing adsorption starting from $\phi = 0.089$, with $\Gamma = 50\tau^{-1}$ (monodisperse GCM samples). The dashed black lines indicate the end of the pseudo-plateau in the particle adsorption and the end of the second particle uptake, respectively. Right: Distributions of particle displacements at times corresponding to the arrows in the left panel. The dashed lines are Gaussian distributions obtained by fitting the whole set of data.

all particles at the interface for IPL and GCM together with the size distribution in the bulk (which is the same for the two interaction potentials). The data indicate a qualitative difference between IPL and GCM: whereas we overall find a shift toward smaller particle sizes as adsorption proceeds, due to the increasing steric hindrances limiting the acceptance of new particle insertion, this effect is clearly much more pronounced in the case of the GCM interaction potential. This striking difference can indeed justify the absence of the pseudo-plateau in the adsorption kinetics of polydisperse samples: the adsorption can proceed via the uptake of small enough particles instead of slowing down until new available space is obtained via the ordering of the interface. To understand the qualitative difference found for the two interaction potentials, we consider that the significantly longer range and weaker spatial variation of the repulsion in the GCM may have an important role, in particular with respect to the relative variation of the particle sizes (for the polydispersity considered here) and their adsorption. Fig. 14 contains two snapshots of polydisperse samples during adsorption for the GCM systems where the color code here indicates the repulsive energy (in units of $k_B T$) that a test particle of size 1.3σ (left, corresponding to the upper end of the particle size distribution) and of size 0.7σ (right, corresponding to the lower end of the particle size distribution) would experience if inserted at that position at a surface coverage $\phi \simeq 0.0975$. The snapshots show sections of the simulation box of size ca. $16\sigma \times 28\sigma$. The Figure shows that indeed in the case of GCM for small particles even when the surface coverage is quite close to its maximum value there are still relatively extended regions where the steric repulsion can be overcome by the adsorption strength ($\simeq 200k_B T$). The large particles, instead, experience a homogeneous net repulsive energy much larger than the adsorption strength. With the IPL interactions one would need a much larger size disparity (and hence size polydispersity) to produce the same energy differences. The emerging picture is therefore that the combination of enhanced softness and longer range in the GCM is responsible for the size selection mechanism which allows for the adsorption to proceed faster in spite of the fact that particle rearrangements at the interface may be severely hindered.

We summarize these findings in Fig. 15, which is a cartoon of the two potentials, where we have highlighted the range to interparticle distance for which the interaction energy is weaker than the adsorption energy of a particle of unit size ($200k_B T$) but still significantly larger than $\simeq k_B T$, the value which we assume is roughly corresponding to crowding at the interface. In the case of the GCM, this range of interparticle distances is quite larger than the variation of the particle sizes with the polydispersity used here ($\simeq 1\sigma$ vs $\simeq 0.6\sigma$), hence the adsorption can proceed without requiring major particle rearrangements at the interface.

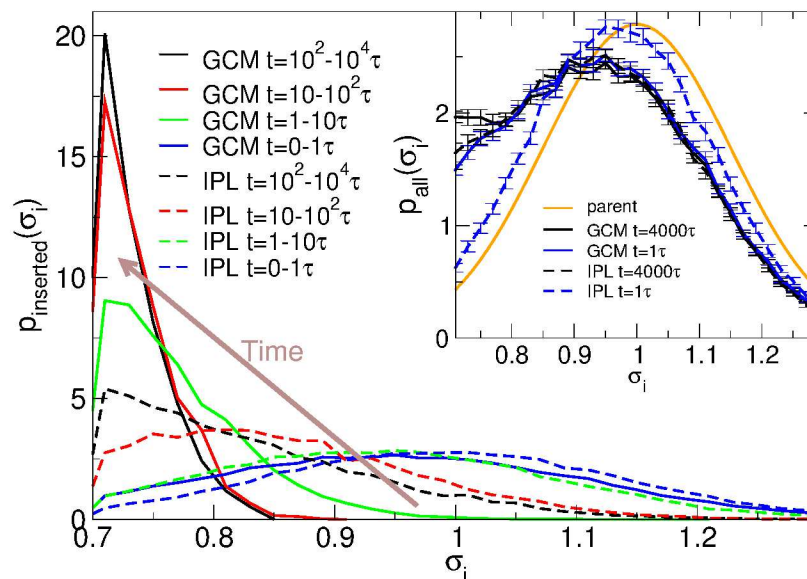


Fig. 13 Size distribution of particles inserted during particular time intervals for IPL (dashed) and GCM (full lines). Inset: Size distribution of all particles present at the interface at a certain time t and the parent distribution in the reservoir (orange).

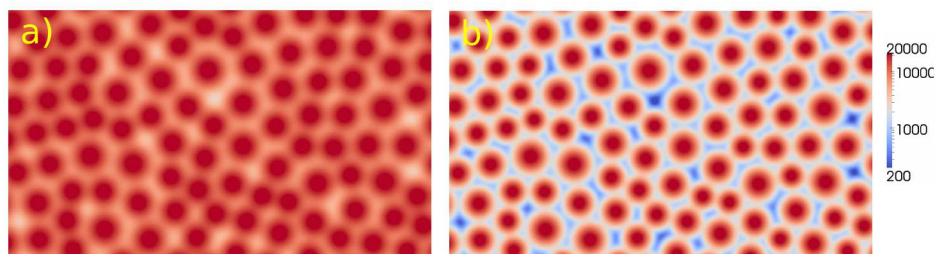


Fig. 14 Snapshots from polydisperse systems during the adsorption process for GCM. The color code corresponds to the repulsion (in units of $k_B T$) experienced by a particle of size 1.3σ (left) and 0.7σ (right) if it were inserted at that particular position at $\phi \simeq 0.0975$. The snapshot corresponds to a section of the simulation box of roughly $16\sigma \times 28\sigma$.

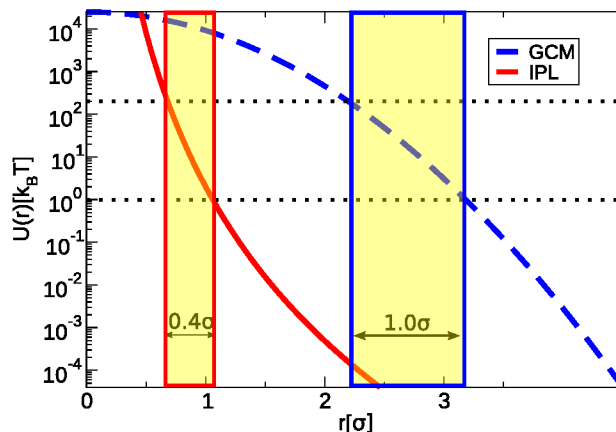


Fig. 15 Comparison of the inverse power law potential (IPL) and the Gaussian Core Model (GCM). The shaded regions mark the the range of particle distances for which adsorption is likely, but particle repulsion is larger than $k_B T$.

In the case of IPL instead, this range is quite narrower, and this feature severely slows down the adsorption unless new suitable space is obtained by increasing the local order at the interface. The irreversible adsorption in IPL systems is therefore likely to be dominated by particle rearrangements at the interface, whereas it may be more easily controlled by size selection mechanisms with ultrasoft interactions.

5 Conclusions

We have performed an extended study of the interplay between the emerging interface dynamics for nanoparticle self-assembly at a liquid interface and the adsorption kinetics. Our investigations have elucidated that in general, in presence of soft repulsive interactions between the nanoparticles at the interface, the crowding of the interface can affect and slow down the adsorption process. Nevertheless we have also found that for ultrasoft interactions, such as the ones that may be induced by the presence of a thick and soft polymer brush grafted on the particle surface, a small size polydispersity may allow for significantly accelerating the adsorption. The origin of this phenomenon is in the fact that a long range and much softer repulsion leads to switching, at high coverages and for a small size polydispersity, from an irreversible adsorption that is essentially limited by the particle rearrangements at the interface to an adsorption that can proceed further by size selection. The same phenomenon could be in principle observed also with steeper repulsive interactions but would require much larger particle size polydispersity to achieve the same effect. In particular, we have been able to rationalize these results by comparing the size polydispersity to the range of interparticle distances over which the repulsion becomes $> k_B T$. These findings suggest that polymer shell nanoparticles might offer new possibilities to better tune the self-assembly at liquid interfaces and design the interface properties, with the absence of a pseudo-plateau in the adsorption kinetics being associated to smaller locally ordered domains. They also call for new, more systematic experimental investigations of these systems.

We have also found that the crowding and the slowing down of the particle motion at the interface is directly coupled to the adsorption kinetics in the case of relatively steep repulsive interactions between the nanoparticles, whereas with ultrasoft interactions the adsorption can proceed even if the particle motion at the

interface is quite close to structural arrest. This would imply, according to our results, that a sudden uptake of new particles due to the ongoing adsorption will tend to trigger fast, avalanche-like particle rearrangements at the interface with steeper repulsive interactions, whereas with much softer interactions the new particle uptake won't perturb significantly the statistics (in terms of rate and spatial extent of the events) of the particle rearrangements. On this basis, combining measurements of relatively large scale particle displacements at the interface with monitoring the adsorption kinetics in experiments with controlled size polydispersity could offer new insight into the effective interactions between the nanoparticles assembled at the liquid interface and their tendency to order. Although the two cases considered here, the IPL and the GCM potential, can be seen as at the two possible extremes for the effective interactions between repulsive nanoparticles at liquid interfaces, recent simulations and experiments have also suggested that in specific solvent conditions the effective interactions may feature a clear separation of length scales (i.e., a shoulder in the interaction potential)²⁴. The outcomes of the numerical study performed here suggest that a rich scenario of different mechanisms governing the adsorption kinetics and the particle dynamics at the interface might emerge also in those cases and motivate further investigations, for both experiments and simulations. Finally, the results discussed here deliver new fundamental understanding that can also be helpful for rationalising more complex situations, ranging from the adsorption of non-spherical nanoparticles to phenomena of competitive or sequential adsorption in multicomponent systems.

Acknowledgements

The authors are indebted to Lucio Isa for many stimulating discussions. This work was supported by the Swiss National Science Foundation (Grant No. PP00P2_126483/1 and PP00P2_150738) and by National Science Foundation under Grant No. NSF PHY11-25915.

References

- 1 M. Grzelczak, J. Vermant, E. M. Furst and L. M. Liz-Marzán, *ACS Nano*, 2010, **4**, 3591–605.
- 2 L. Isa, K. Kumar, M. Müller, J. Grolig, M. Textor and E. Reimhult, *ACS Nano*, 2010, **4**, 5665–70.
- 3 F. Bresme and M. Oettel, *J. Phys. Condens. Matter*, 2007, **19**, 413101.
- 4 W. H. Binder, *Angew. Chem. Int. Ed. Engl.*, 2005, **44**, 5172–5.
- 5 A. Böker, J. He, T. Emrick and T. P. Russell, *Soft Matter*, 2007, **3**, 1231.
- 6 N. Popp, S. Kutuzov and A. Böker, *Phys. Chem. Chem. Phys.*, 2010, 39–58.
- 7 A. Nelson, D. Wang, K. Koynov and L. Isa, *Soft Matter*, 2014, **11**, 118–29.
- 8 Z. Nie, A. Petukhova and E. Kumacheva, *Nat. Nanotechnol.*, 2010, **5**, 15–25.
- 9 L. Isa, E. Amstad, M. Textor and E. Reimhult, *Chim. Int. J. Chem.*, 2010, **64**, 145–149.
- 10 L. Isa, E. Amstad, K. Schwenke, E. Del Gado, P. Ilg, M. Kröger and E. Reimhult, *Soft Matter*, 2011, **7**, 7663–7675.
- 11 K. Schwenke, L. Isa and E. Del Gado, *Langmuir*, 2014, **30**, 3069–74.
- 12 Z. A. Zell, L. Isa, P. Ilg, L. G. Leal and T. M. Squires, *Langmuir*, 2014, **30**, 110–9.
- 13 M. Cui, T. Emrick and T. P. Russell, *Science*, 2013, **342**, 460–463.
- 14 D. A. Wood, C. D. Santangelo and A. D. Dinsmore, *Soft Matter*, 2013, **9**, 10016–10024.
- 15 A. D. Law, M. Auriol, D. Smith, T. S. Horozov and D. M. A. Buzza, *Phys. Rev. Lett.*, 2013, **110**, 138301.
- 16 G. B. Davies, T. Krüger, P. V. Coveney, J. Harting and F. Bresme, *Advanced Materials*, 2014, **26**, 6715–6719.
- 17 W. Li, P. F. Nealey, J. J. de Pablo and M. Müller, *Phys. Rev. Lett.*, 2014, **113**, 168301.
- 18 E. Bianchi, C. N. Likos and G. Kahl, *Nano Letters*, 2014, **14**, 4196–4196.
- 19 J. A. Fan, C. Wu, K. Bao, J. Bao, R. Bardhan, N. J. Halas, V. N. Manoharan, P. Nordlander, G. Shvets and F. Capasso, *Science*, 2010, **328**, 1135–8.
- 20 J. A. Labastide, M. Baghgar, I. Dujovne, Y. Yang, A. D. Dinsmore, B. G. Sumpter, D. Venkataraman and M. D. Barnes, *The Journal of Physical Chemistry Letters*, 2011, **2**, 3085–3091.
- 21 E. R. Chen, D. Klotsa, M. Engel, P. F. Damasceno and S. C. Glotzer, *Phys. Rev. X*, 2014, **4**, 011024.
- 22 J. Broughton, G. Gilmer and J. Weeks, *Phys. Rev. B*, 1982, **25**, 4651–4669.
- 23 M. Hurley and P. Harrowell, *Phys. Rev. E*, 1995, **52**, 1694.

-
- 24 K. Schwenke, L. Isa, D. L. Cheung and E. Del Gado, *Langmuir*, 2014, **30**, 12578–86.
- 25 F. Lo Verso, L. Yelash, S. a. Egorov and K. Binder, *J. Chem. Phys.*, 2011, **135**, 214902.
- 26 T. Gillich, C. Acikgöz, L. Isa, A. D. Schlüter, N. D. Spencer and M. Textor, *ACS Nano*, 2013, **7**, 316–29.
- 27 B. Binks and J. Clint, *Langmuir*, 2002, **18**, 1270–1273.
- 28 B. P. Binks, *Curr. Opin. Colloid Interface Sci.*, 2002, **7**, 21–41.
- 29 F. van Swol, L. V. Woodcock and J. Neil Cape, *J. Chem. Phys.*, 1980, **73**, 913.
- 30 J. J. Cerdà, T. Sintes and R. Toral, *Macromolecules*, 2003, **36**, 1407–1413.
- 31 S. Prestipino, F. Saija and P. V. Giaquinta, *J. Chem. Phys.*, 2005, **123**, 144110.
- 32 S. Prestipino, F. Saija and P. V. Giaquinta, *Phys. Rev. Lett.*, 2011, **106**, 235701.
- 33 A. Ikeda and K. Miyazaki, *Phys. Rev. Lett.*, 2011, **106**, 015701.
- 34 P. Mausbach, A. Ahmed and R. J. Sadus, *J. Chem. Phys.*, 2009, **131**, 184507.
- 35 A. Ikeda and K. Miyazaki, *J. Chem. Phys.*, 2011, **135**, 024901.
- 36 R. Colin, A. M. Alsayed, J.-C. Castaing, R. Goyal, L. Hough and B. Abou, *Soft Matter*, 2011, **7**, 4504.
- 37 G. M. Hocky, D. Coslovich, A. Ikeda and D. R. Reichman, *Phys. Rev. Lett.*, 2014, **113**, 157801.
- 38 D. M. Mitrinović, A. M. Tikhonov, M. Li, Z. Huang and M. L. Schlossman, *Phys. Rev. Lett.*, 2000, **85**, 582–5.
- 39 A. Poynor, L. Hong, I. Robinson, S. Granick, Z. Zhang and P. Fenter, *Phys. Rev. Lett.*, 2006, **97**, 1–4.
- 40 P. Pieranski, *Phys. Rev. Lett.*, 1980, **45**, 569–572.
- 41 A. Stocco, T. Mokhtari, G. Haseloff, A. Erbe and R. Sigel, *Phys. Rev. E*, 2011, **83**, 1–11.
- 42 D. Wang, S. Yordanov, H. M. Paroor, A. Mukhopadhyay, C. Y. Li, H.-J. Butt and K. Koynov, *Small*, 2011, **7**, 3502–3507.
- 43 M. R. Oberholzer, N. J. Wagner and A. M. Lenhoff, *J. Chem. Phys.*, 1997, **107**, 9157.
- 44 J. J. Gray and R. T. Bonnecaze, *J. Chem. Phys.*, 2001, **114**, 1366.
- 45 S. Watanabe, M. Miyahara and K. Higashitani, *J. Chem. Phys.*, 2005, **122**, 104704.
- 46 B. Widom, *J. Chem. Phys.*, 1963, **39**, 2808.
- 47 D. Frenkel and B. Smit, *Understanding Molecular Simulation*, Academic press, 2002.
- 48 N. B. Wilding and P. Sollich, *J. Chem. Phys.*, 2002, **116**, 7116.
- 49 G. Martyna, M. Tuckerman, D. Tobias and M. Klein, *Mol. Phys.*, 1996, **87**, 1117–1157.
- 50 K. Du, E. Glogowski, T. Emrick, T. P. Russell and A. D. Dinsmore, *Langmuir*, 2010, **26**, 12518–12522.
- 51 P. S. Clegg, E. M. Herzig, A. B. Schofield, S. U. Egelhaaf, T. S. Horozov, B. P. Binks, M. E. Cates and W. C. K. Poon, *Langmuir*, 2007, **23**, 5984–5994.
- 52 D. Nelson, *Defects and Geometry in Condensed Matter Physics*, Cambridge University Press, Cambridge, 2002.
- 53 L. Berthier, G. Biroli, J.-P. Bouchaud, L. Cipelletti and W. Van Saarloos, *International Series of Monographs on Physics*, 2011.
- 54 M. M. Hurley and P. Harrowell, *J. Chem. Phys.*, 1996, **105**, 10521.
- 55 D. N. Perera and P. Harrowell, *J. Chem. Phys.*, 1999, **111**, 5441.
- 56 T. Gleim, W. Kob and K. Binder, *Phys. Rev. Lett.*, 1998, **81**, 4404–4407.
- 57 A. Rahman, *Phys. Rev.*, 1964, **136**, A405–A411.
- 58 W. Kob, C. Donati, S. Plimpton, P. Poole and S. Glotzer, *Phys. Rev. Lett.*, 1997, **79**, 2827–2830.
- 59 E. R. Weeks, J. C. Crocker, A. C. Lewitt, A. B. Schofield and D. A. Weitz, *Science*, 2000, **287**, 627–631.
- 60 T. Narumi, S. V. Franklin, K. W. Desmond, M. Tokuyama and E. R. Weeks, *Soft Matter*, 2011, **7**, 1472.
- 61 R. Zangi and S. Rice, *Phys. Rev. Lett.*, 2004, **92**, 035502.
- 62 E. Sanz, C. Valeriani, E. Zaccarelli, W. C. K. Poon, M. E. Cates and P. N. Pusey, *Proceedings of the National Academy of Sciences*, 2014, **111**, 75–80.
- 63 Y. Rahmani, K. van der Vaart, B. van Dam, Z. Hu, V. Chikkadi and P. Schall, *Soft Matter*, 2012, **8**, 4264.